 CMES, vol.1516, no.1, pp.1-25, 2009

Modelling Elasto-Plasticity Using the Hybrid MLPG Method

Claire Heaney[1,2], Charles Augarde[2] and Andrew Deeks[2]

Abstract: Meshless methods continue to generate strong interest as alternatives to conventional finite element methods. One major area of application as yet relatively unexplored with meshless methods is elasto-plasticity. In this paper we extend a novel numerical method, based on the Meshless Local Petrov-Galerkin (MLPG) method, to the modelling of elasto-plastic materials. The extended method is particularly suitable for problems in geomechanics, as it permits inclusion of infinite boundaries, and is demonstrated here on footing problems. The current usage of meshless methods for problems involving plasticity is reviewed and guidance is provided in the choice of various modelling parameters.

Keywords: meshless, meshfree, elasto–plasticity, meshless local Petrov–Galerkin

1 Introduction

Problems requiring modelling with elasto–plasticity routinely arise in many areas of engineering, two prominent examples being metal–forming and geotechnical engineering. In the former the boundary conditions are often prescribed and the quantity of interest is the work required to complete a given manufacturing operation. In the latter predictions of movements or of instability are required for domains which are generally kinematically less–constrained, and where initial stresses due to self–weight must sometimes be considered. There is also a considerable body of literature on micromechanical material modelling using numerical methods to study crystal plasticity requiring similar models. In all of the above robust finite element (FE) modelling is now well–tested and available in a number of commercial packages. Where finite elements currently struggle are with challenging problems that are beginning to be of interest to practising engineers. In particular there is an increasing desire to model in 3D, which leads to a disproportionate overhead in

[1] Corresponding author. Tel: +44 191 334 2487; Fax: +44 191 334 2407; Email: claire.heaney@dur.ac.uk

[2] School of Engineering and Computing Sciences, Durham University, Durham DH1 3LE, UK

meshing. There are also problems for which finite deformation must be modelled and remeshing is required during an analysis to ensure accuracy. In geotechnical engineering 3D models are required to accurately predict movements due to tunnelling operations (e.g. Kasper and Meschke (2004)) whilst finite deformation is needed to model penetration problems found in site investigation (Sheng, Nazem, and Carter, 2009). Many examples exist of 3D finite deformation modelling for micromechanics of crystalline materials, a recent example being Wang, Daniewicz, Horstemeyer, Sintay, and Rollett (2009). To avoid the difficulties of using finite elements, some researchers have begun to focus on "meshless" or "meshfree" methods which discretise a problem without requiring a mesh. Adaptive refinement of a meshless domain is a matter of adding nodes, a far simpler operation than remeshing with elements, especially for 3D. While there are currently drawbacks to their use, which will be discussed below, it remains possible that in the future these methods will challenge finite elements for demanding problems of the types mentioned above.

Meshless methods for solid mechanics were originally derived from work in the 1980s on smoothed–particle hydrodynamics (SPH) by Monaghan and co–workers (Monaghan, 1988) which has been shown to be viable for dynamic simulations but less so for statics due to boundary problems. The meshless methods most widely used in solid mechanics today are the Element–Free Galerkin (EFG) method (Belytschko, Lu, and Gu, 1994) and the Meshless Local Petrov–Galerkin (MLPG) method (Atluri and Zhu, 1998). These methods have their origins in the work by Nayroles, Touzot, and Villon (1992) which introduced the idea of discretisation of a problem domain by a nodal distribution and a boundary definition alone, where the field variable is approximated by approximants to nodal values. Construction of these approximants requires only nodes and no mesh of elements, and is based on a "moving least squares" (MLS) approach in which nodes influence zones of "support" around their locations. These approximants had already been suggested by Lancaster and Salkauskas (1981) for use in other applications such as surface reconstruction. A major advantage of these meshless methods is that the solutions and their derivatives are smooth thus no post–processing is required to obtain a smooth stress field unlike in conventional FE approaches. The difference between the EFG and MLPG methods is that the former requires the generation of background integration cells. The latter does not as integrations (to provide terms in the stiffness matrix for instance) are carried out over local domains around each node. It can be said therefore that the MLPG method is truly meshless (Atluri and Zhu, 1998) and that is the meshless technique used here. Over the last decade a bewildering array of variations on EFG and MLPG, as well as other meshless methods, have been proposed for use in solid mechanics e.g. Atluri, Liu, and Han

(2006). General surveys of methods can be found in Fries and Matthies (2004) and, most recently, in Nguyen, Rabczuk, Bordas, and Duflot (2008). Recent publications show considerable interest in development of the MLPG method for a range of problems and physics in analysis of solids such as fracture (Feng, Han, and Li, 2009; Sladek, Sladek, Solek, and Pan, 2008), plates (Jarak and Soric, 2008; Sladek, Sladek, Krivacek, Wen, and Zhang, 2007), finite deformation (Batra and Porfiri, 2008; Han, Rajendran, and Atluri, 2005), vibrations (Andreaus, Batra, and Porfiri, 2005), intelligent materials (Sladek, Sladek, Solek, and Atluri, 2008) and poroelasticity (Bergamaschi, Martinez, and Pini, 2009). While many publications are confined to 2D models the MLPG method is straightforward to extend to 3D as demonstrated in a number of references (Han and Atluri, 2004; Pini, Mazzia, and Sartoretto, 2008; Sladek, Sladek, and Solek, 2009; Sladek, Sladek, Solek, Tan, and Zhang, 2009) However, development of the MLPG method, and indeed the EFG method, for problems with material nonlinearity (e.g. elasto-plasticity) has to date been limited.

The majority of papers in which meshless methods are applied to problems of elasto–plasticity use the EFG method and are confined to continuum modelling problems rather than micromechanics. Barry and Saigal (1999) describe the formulation for incremental elasto–plasticity in detail, demonstrating it not to differ markedly from the FE approach. They then give examples of use for elastic problems and two elasto–plastic problems. Their conclusions, as in most other papers, indicate that the choice of nodal support to be of prime importance for the robustness of a meshless elasto–plastic formulation. The same point is made in other papers concerning elasto–plastic continua (Kargarnovin, Toussi, and Fariborz, 2004; Hazama, Okuda, and Wakatsuchi, 2001) and plates (Belinha and Dinis, 2006) but few details are provided. Askes and co–workers have produced a number of papers in this area linking the issue of nodal support to locking seen in perfect plasticity (Askes, de Borst, and Heeres, 1999), implementation of constraints (Pannachet and Askes, 2000) and in gradient plasticity formulations (Pamin, Askes, and de Borst, 2003). A rare example of the use of an alternative to the EFG method is given in Wu, Chen, Chi, and Huck (2001), where the Reproducing Kernel Particle method (Liu, Jun, Li, Adee, and Belytschko, 1995) is used to model elasto–plastic problems. A search of the published literature reveals only three papers that discuss modelling elasto–plasticity with the MLPG method. Xiong, Long, Liu, and Li (2006) give results for a cantilever beam using a uniform nodal arrangement and compare their results with FEM simulations. Long, Liu, and Li (2008) model elasto–plastic fracture problems using an MLPG method with a Heaviside test function and compare their results with predictions of linear elastic fracture mechanics and also ANSYS. However neither of these provide insight or guidance in the use of MLPG with material nonlinearity. Soares, Sladek, and Sladek (2009) presents recent work on analysis of dynamic problems including one example with elasto-plasticity.

As well as the concentration on the EFG method, in all of the references cited above, uniform distributions of nodes are used which make the conclusions drawn thus far of reduced use for unstructured nodal arrangements, perhaps derived from an adaptive procedure. The purpose of this paper is to introduce an extension to an MLPG-based method to model elasto-plastic materials highlighting some issues that arise relating mainly to nodal distributions and choice of support rules, which will help those wishing to employ this exciting method for elasto–plastic modelling.

The paper is organized as follows. In §2 the shape functions for moving least–squares based meshless methods are derived and then used in a weighted residual approach for elasto–plastic solids. This yields a linear system in which the displacements are unknowns, highlighting the similarities to this derivation and that arising from the FE method. In §3 we introduce a recently developed hybrid MLPG method that deals with infinite domains commonly found in geotechnics and develop it to model elasto-plasticity. Some implementation issues related to the hybrid method are discussed and guidance is then giving on choices of modelling parameters to achieve good results.

2 Meshless methods based on moving least–squares

2.1 Shape functions

The EFG and MLPG methods are meshless in the sense that no elements are needed. However elements are replaced in these methods by the concept of zones of “support" around each node. As with FE methods, shape functions can be derived from each node in the domain and, in these methods, are arrived at via a moving least squares (MLS) approach which is now described. Each node’s support is the subdomain in which that node influences the approximation (usually in a symmetrically weighted sense). Typical weight functions used are truncated splines and exponentials, which are smooth and continuous, meaning that the MLS–based shape functions are also smooth and continuous to a higher order than standard FE functions.

The MLS approximation to a set of n nodal data points $\mathbf{U} = \{u_I, \mathbf{x}_I\}, I = 1,2,\ldots,n$ can be constructed as

$$u^h(\mathbf{x}) = \sum_{I=1}^{n} \phi_I(\mathbf{x}) u_I = \mathbf{\Phi}^T(\mathbf{x})\mathbf{u} \tag{1}$$

where $u^h(\mathbf{x})$ denotes the approximate value of $u(\mathbf{x})$, n is the number of nodes in support at $\mathbf{x}$ and $\phi_I(\mathbf{x})$ is the shape function of node I at $\mathbf{x}$. $\Phi^T(\mathbf{x})$ is a $1 \times n$ matrix collecting together the shape functions ϕ_I and $\mathbf{u}$ is a vector containing the fictitious nodal values. As in the FE method if $u(\mathbf{x})$ is approximated as a polynomial then

$$u^h(\mathbf{x}) = \sum_{j=1}^{m} p_j(\mathbf{x})a_j(\mathbf{x}) = \mathbf{p}^T(\mathbf{x})\mathbf{a}(\mathbf{x}) \tag{2}$$

where m is the number of monomials in the basis matrix $\mathbf{p}(\mathbf{x})$, e.g. $m = 3$ for a linear basis in 2D or a quadratic basis in 1D, and $\mathbf{a}(\mathbf{x})$ is a vector of coefficients. In the MLS approximation, the shape functions are obtained by minimizing a weighted residual J to determine the coefficients $\mathbf{a}(\mathbf{x})$ where

$$J(\mathbf{x}) = \sum_{I=1}^{n} w_I(\mathbf{x}) \left[\mathbf{p}^T(\mathbf{x}_I)\mathbf{a}(\mathbf{x}) - u_I\right]^2 \tag{3}$$

where $w_I(\mathbf{x}) \equiv w(\mathbf{x} - \mathbf{x}_I)$ is the weight function for node I evaluated at point $\mathbf{x}$. Minimizing J leads to the following

$$\mathbf{A}(\mathbf{x})\mathbf{a}(\mathbf{x}) = \mathbf{B}(\mathbf{x})\mathbf{u} \tag{4}$$

where the elements of matrix $\mathbf{A}(\mathbf{x})_{m\times m}$ are given by

$$A_{jk} = \sum_{I=1}^{n} w_I(\mathbf{x})p_j(\mathbf{x}_I)p_k(\mathbf{x}_I) \quad j,k = 1,\ldots,m \tag{5}$$

and the elements of matrix $\mathbf{B}(\mathbf{x})_{m\times n}$ by

$$B_{jI} = w_I(\mathbf{x})p_j(\mathbf{x}_I) \quad j = 1,\ldots,m, I = 1,\ldots,n. \tag{6}$$

The coefficients $\mathbf{a}(\mathbf{x})$ can be found from (4) by inverting $\mathbf{A}(\mathbf{x})$

$$\mathbf{a}(\mathbf{x}) = \mathbf{A}^{-1}(\mathbf{x})\mathbf{B}(\mathbf{x})\mathbf{u},$$

so (2) becomes

$$u^h(\mathbf{x}) = \mathbf{p}(\mathbf{x})^T\mathbf{A}^{-1}(\mathbf{x})\mathbf{B}(\mathbf{x})\mathbf{u} \tag{7}$$

and the shape functions are found, by comparison with Eqn (1), as

$$\Phi = \mathbf{p}^T\mathbf{A}^{-1}\mathbf{B} \tag{8}$$

where the dependence on $\mathbf{x}$ for all terms has been removed for clarity. The derivatives of the shape functions can be found as

$$\Phi_{,k} = \mathbf{p}_{,k}^T\mathbf{A}^{-1}\mathbf{B} + \mathbf{p}^T\left(\mathbf{A}_{,k}^{-1}\mathbf{B} + \mathbf{A}^{-1}\mathbf{B}_{,k}\right) \tag{9}$$

where k denotes the coordinate index and

$$\mathbf{A}_{,k}^{-1} = -\mathbf{A}^{-1}\mathbf{A}_{,k}\mathbf{A}^{-1}. \tag{10}$$

A and **B** can be written in matrix form as

$$\mathbf{A} = \mathbf{P}^T\mathbf{W}\mathbf{P} \tag{11a}$$

$$\mathbf{B} = \mathbf{P}^T\mathbf{W} \tag{11b}$$

where **P** is an $n \times m$ matrix defined by

$$\mathbf{P} = \begin{bmatrix} \mathbf{p}(\mathbf{x}_1) \\ \mathbf{p}(\mathbf{x}_2) \\ \vdots \\ \mathbf{p}(\mathbf{x}_n) \end{bmatrix} \tag{12}$$

and **W** is an $n \times n$ diagonal matrix

$$\mathbf{W} = [\ diag(w_1(\mathbf{x}), \ldots, w_n(\mathbf{x}))\ ]_{n\times n}. \tag{13}$$

The MLS procedure leads to an approximation u^h rather than an interpolation. The shape functions therefore do not possess the delta property of conventional finite element functions.

2.2 Formation of the stiffness matrix

Having obtained the shape functions, the procedure to obtain the stiffness matrix for the problem is similar to that for the FEM. Dealing with the elastic behaviour first, assuming a domain Ω with boundary Γ and writing in matrix–vector format, the strong form of equilibrium (in the absence of body forces) is

$$\mathbf{L}^T\sigma \quad = \quad \mathbf{0} \tag{14}$$

where **L** is the differential operator and σ the components of the stress tensor in Voigt notation. Essential boundary conditions are defined as

$$\mathbf{u}^h = \bar{\mathbf{u}} \ \text{ on } \ \Gamma_u. \tag{15}$$

The weak form is obtained by multiplying by a test function **v** as follows

$$\int_\Omega \mathbf{v}^T \left(\mathbf{L}^T\sigma\right)\, d\Omega = 0. \tag{16}$$

Using the Green–Gauss theorem Eqn (16) can be converted to

$$\int_{\Omega} (\mathbf{L}\mathbf{v})^T \sigma \, d\Omega - \int_{\Gamma_t} \mathbf{v}^T \bar{\mathbf{t}} \, d\Gamma = 0. \tag{17}$$

where $\bar{\mathbf{t}}$ are the surface tractions and the domain boundary $\Gamma = \Gamma_u \cup \Gamma_t$. Since the shape functions do not possess the delta property, essential boundary conditions cannot be imposed directly. Instead indirect imposition is necessary by penalty approach, Lagrange multipliers, Nitsche's method or via coupling to finite elements on the boundary (Fernández-Méndez and Huerta, 2004). In this study we use the first of these methods and the weak form including imposition of essential boundary conditions becomes

$$\int_{\Omega} (\mathbf{L}\mathbf{v})^T \sigma \, d\Omega - \int_{\Gamma_t} \mathbf{v}^T \bar{\mathbf{t}} \, d\Gamma + \alpha \int_{\Gamma_u} \mathbf{v}^T \left(\mathbf{u}^h - \bar{\mathbf{u}} \right) \, d\Gamma = 0 \tag{18}$$

where α is a user–defined penalty parameter. Discretisation of Eqn (18) leads to the linear system

$$\mathbf{K}\mathbf{u} = \mathbf{f} \tag{19}$$

where

$$\mathbf{K} = \int_{\Omega} \mathbf{B}_v^T \mathbf{D} \mathbf{B} \, d\Omega + \alpha \int_{\Gamma_u} \mathbf{v}^T \Phi \, d\Gamma \tag{20}$$

$$\mathbf{f} = \alpha \int_{\Gamma_u} \mathbf{v}^T \bar{\mathbf{u}} \, d\Gamma + \int_{\Gamma_t} \mathbf{v}^T \bar{\mathbf{t}} \, d\Gamma \tag{21}$$

$$\tag{22}$$

in which $\mathbf{B}_v$ and $\mathbf{B}$ are matrices of derivatives of the test and shape functions respectively, $\mathbf{D}$ is the elastic constitutive matrix and $\mathbf{f}$ is the force vector formed from the penalty terms at essential boundaries and the tractions $\bar{\mathbf{t}}$ at natural boundaries. The choice of test function can be identical to the shape function, i.e. $\mathbf{B}_v = \mathbf{B}$, yielding the Element Free Galerkin (EFG) method (Belytschko, Lu, and Gu, 1994), or be taken from another space entirely, yielding the Meshless Local Petrov–Galerkin (MLPG) method, i.e. $\mathbf{B}_v \neq \mathbf{B}$ (Atluri and Zhu, 1998; Fries and Matthies, 2004). In the MLPG method the integrations in Eqns (19) and (20) are carried out over test domains and their boundaries local to each node.

2.3 Choice of nodal arrangement and size of zones

One of the most important issues in the MLPG method is choice of nodal arrangement and support and test zones. We will later show this to be of major significance in modelling elasto-plasticity. Uniform nodal arrangements are the most attractive to modellers and the choice of nodal arrangement is strongly linked to the rule for determining the support zones and test zones around each node. The former is set by the nature of the weighting function w_I, which in this study was a quartic spline function

$$w_I(\mathbf{x}) = \begin{cases} 1-6\left(\frac{d_I}{r_{supp}}\right)^2+8\left(\frac{d_I}{r_{supp}}\right)^3-3\left(\frac{d_I}{r_{supp}}\right)^4 & 0 \leqslant d_I < r_{supp} \\ 0 \quad d_I \geqslant r_{supp} \end{cases} \tag{23}$$

This function has a value of unity at node I and then decays smoothly to zero a radius r_{supp} from the node. ($d_I \equiv |\mathbf{x}-\mathbf{x}_I|$ is the distance of the point $\mathbf{x}$ to node I). The test function determines the local zone around each node in which the weak form is satisfied and, as in previous work, the test function used here is identical to w_I above with r_{supp} replaced by a smaller test radius r_{test}. In Atluri and Shen (2002) both are set to be proportional to the distance from the node in question to its nearest neighbour (d_{min}):

$$r_{supp} = a\,d_{min} \qquad\qquad r_{test} = b\,d_{min}\,, \tag{24}$$

where a and b are chosen by the user and are usually within the range $[0.5, 5.0]$. The choice of a is governed by the nodal arrangement, the dimension of the problem and the order of the monomial basis, whereas the choice of b depends only on the nodal arrangement. The range for a is large, and choice of an optimal value is problem dependent. There is little firm guidance in the literature on suitable values since they depend on the given problem and the nodal distribution. Therefore it is necessary to experiment with a range of values for each problem (in the same way that a range of meshes should be used in the FEM).

The test radius must be large enough so that the domain is completely covered by the union of all the test domains (in this case circles of radius r_{test}). This ensures that the weak form of the governing equations is satisfied throughout the domain. For uniform arrangements of nodes the minimum value of r_{test} can be calculated in advance and will be the same for all nodes ($r_{test} \geqslant d_{min}/\sqrt{2}$). For non–uniform grids the minimum value of r_{test} is not known *a priori*. The authors have found that setting r_{test} to be larger than the minimum value gives better results. This is discussed further in §3.2.

As stated in §2.1 the support radius determines the area over which a node influences the solution. Increasing the support radius means that a node will affect the solution over a larger area, and also leads to more couplings between the nodes in the stiffness matrix. As with the test radius, there is a minimum value for the support radius, based on the requirement that there must be at least m nodes in support of each (integration) point. If this is not satisfied the inverse of matrix **A** cannot be calculated (see (8)). However the support radius should also be small enough so that it can model the local behaviour of the solution. Some previous studies take a different approach, which is, to determine the radius of support for each node from a pre–defined, 'ideal' number of supporting nodes for each point in the domain. In Barry and Saigal (1999) the support radii were based on observations that for a quadratic basis a minimum of 27 nodes should be in support of any integration point in the domain, while in more recent work Sterk and Trobec (2008) carry out an extensive study of support radii rules based on this idea and to find which give accurate results for certain example problems. General advice relating to the MLS approximation itself can be found in Nie, Atluri, and Zuo (2006) and Zhuang and Augarde (2010).

3 An elasto–plastic hybrid MLPG method

Deeks and Augarde (2007) describes a novel hybrid MLPG method in which the near field of a problem is modelled with the MLPG method and the far-field with a meshless scaled boundary method, originally described in Deeks and Augarde (2005). This arrangement permits correct modelling of an infinite elastic far-field thus removing the need to decide on location of boundaries. It is particularly useful for geomechanical analyses, such as for foundations, tunnels and slopes, where serious errors can result from inadequately located boundaries. Deeks and Augarde (2007) describes the means by which correct coupling is achieved between the MLPG near field and the scaled boundary far field, which will not be revisited here. As an example of how the hybrid method works Figure 1 shows the arrangement of the two subdomains for the classic 2D plane strain footing problem (closely related to Prandtl's problem) which will be used later in the paper. In the original description of the hybrid MLPG method both subdomains were limited to elastic behaviour only. Here we present results to show the behaviour of a new hybrid MLPG formulation in which elasto-plasticity is incorporated into the MLPG near field (as outlined in the previous section) while the meshless scaled boundary subdomain remains elastic.

Beginning from the elastic formulation of (20) and (21) plasticity can be implemented with an incremental-iterative scheme in the MLPG in the same way as for the FEM and as described in many texts. In the following we use dot notation to indicate infinitesimal or rate quantities. For associated flow and perfect plasticity, the classical theory of plasticity is based on the following assumptions:

(i) additive decomposition of total strain into elastic and plastic parts
$\dot{\varepsilon} = \dot{\varepsilon^e} + \dot{\varepsilon^p}$;

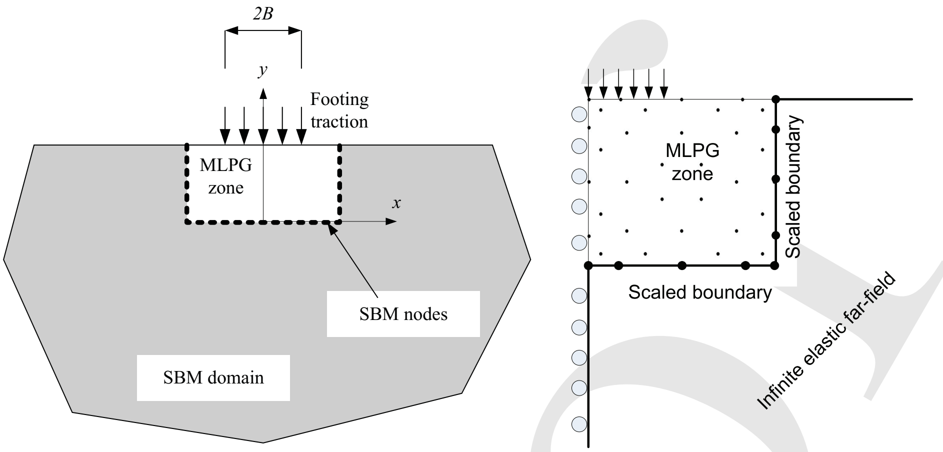

(a) The whole problem

(b) The discretised section, taking account of symmetry

Figure 1: The hybrid meshless scaled boundary method for the footing problem

(ii) a hypoelastic law
$\dot{\sigma} = \mathbf{D}^e \dot{\varepsilon^e}$;

(iii) the associated flow rule (with plastic multiplier $\dot{\lambda}$)

$$\dot{\varepsilon^p} = \dot{\lambda}\,\frac{\partial f}{\partial \sigma} \;;$$

(iv) the Karush-Kuhn-Tucker loading conditions
$f \leqslant 0, \quad \dot{\lambda} \geqslant 0, \quad \dot{\lambda} f = 0$;

(v) the consistency condition
$\dot{\lambda}\dot{f} = 0$ (applied if $f = 0$) .

Throughout this study we use the Prandtl–Reuss constitutive model, which comprises a von Mises yield function with perfect plasticity and associated flow. The von Mises yield function has the form

$$f = \sqrt{J_2} - c_u \;,$$

where J_2 is the second invariant of the deviatoric stress tensor and c_u is the undrained shear strength of the material. To solve equations (i)–(v) the Closest Point Projection (CPP) method is used, which is widely adopted within elasto-plasticity (Simo and Hughes, 1998). For this particular constitutive model the CPP reduces to the radial return method. Linearising the CPP algorithm leads to the so–called algorithmic or consistent tangent $\mathbf{D}^{alg}$. When forming the stiffness matrix, the use of this tangent allows asymptotic quadratic convergence of the global Newton Raphson algorithm.

3.1 Results for elasto-plasticity with uniform nodal arrangements

The effects of using a uniform nodal arrangement for elasto-plastic modelling using the hybrid MLPG method is investigated using a large number of analyses of the footing problem. One half of the problem is modelled due to symmetry (see Figure 1(b)) and load–control used throughout (i.e. a flexible footing). The material properties adopted for the uniform material are Young's modulus $E = 1000$, Poisson's ratio $\nu = 0.25$ and undrained shear strength $c_u = 0.3$ in compatible units. (The radius of the von Mises cylinder is $\sqrt{2}c_u$.) The size of the MLPG domain in all cases is 3×3 units. The results are compared to the analytical solution of a limit load of $(\pi + 2)c_u$ for the related problem of a rigid footing. Referring to the work of Prandtl and Hencky, Hill (1950) develops this solution in regard to an indentation problem for a perfectly plastic–rigid material. This solution therefore acts only as a guide, since, in our examples, we model a flexible footing impinging on an elasto–perfectly–plastic material. The analytical limit load $(\pi + 2)c_u$ applies to a von Mises material of radius $\sqrt{2}c_u$ ("inner von Mises cylinder"). Analytical solutions for footing problems with different materials and boundary conditions can be found in a number of references, e.g. Seyrafian, Gatmiri, and Noorzad (2007). Load–displacement plots for the footing problem (using load–control) for a uniform nodal arrangement are shown in Figure 2(a). The limit load for this problem is taken to be close to the normalised analytical solution for the rigid footing problem of $(\pi + 2)$ given in §3.1. It is clear that for this arrangement it is impossible to get very close to the expected solution. For a nodal support rule where more nodes contribute to the approximation at a point $(a = 4.0)$ convergence is poorer than for a rule with a more local approximation $(a = 3.0)$. The errors seen with the uniform grid can be explained with reference to the manner in which the nodal supports combine. Points near the domain boundaries will have fewer nodes in support than points in the centre of the domain, and consequently the approximation in the centre will be richer than that near the boundaries. This mismatch then leads to errors in stress updates at the boundaries which accumulate until the problem cannot converge.

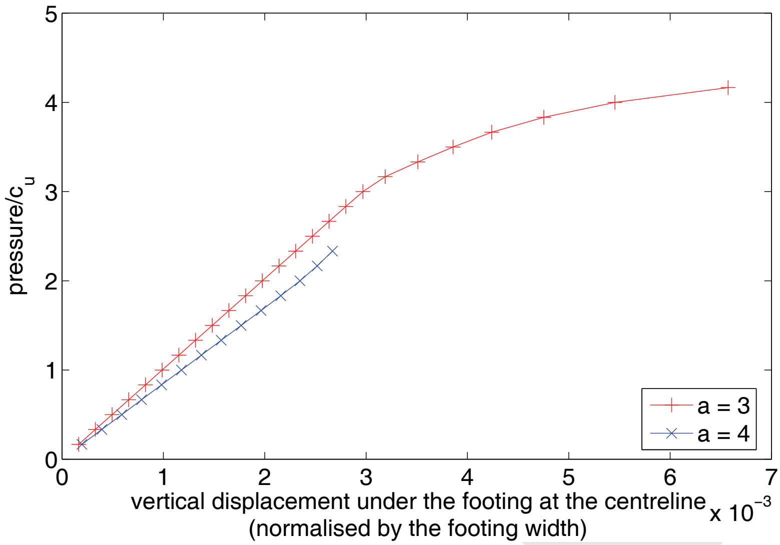

(a) Uniform nodal arrangement

Figure 2: Load displacement curves for uniform nodal arrangement.

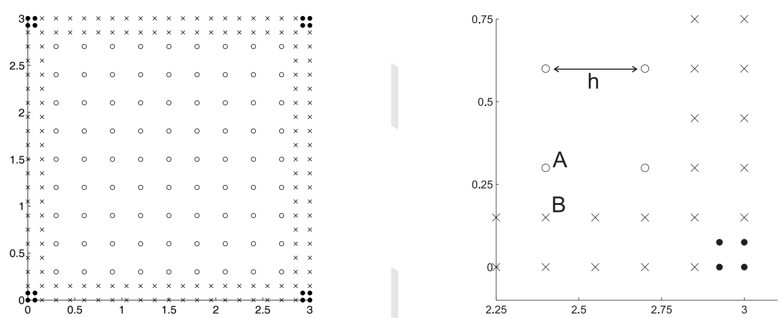

(a) (b)

Figure 3: The hierarchical nodal arrangement, for 233 nodes (266 nodes in total). For a spacing of h in the centre of the domain, the support radius for '∘' nodes is ah, for '×' nodes is $ah/2$, and for '•' nodes is $ah/4$, where a is the factor in Eqn (24).

3.2 A hierarchical nodal arrangement and support rule

In the arrangement described above a set rule for the nodal support is used throughout the domain. Here we show that varying the rule for support radius depending on proximity to a boundary has a major effect on the performance of this meshless method for elasto–plasticity, whilst still allowing a degree of structure to the nodal layout. We term this arrangement "hierarchical" and it is constructed in a manner reminiscent of h–adaptivity in the FEM. A uniform nodal arrangement is first generated with a spacing h. Extra nodes are then added around the boundaries with spacings $h/2$ and $h/4$ (see Figure 3). Adding extra nodes would ordinarily decrease the support radius for some of the h–spaced nodes by a straightforward application of the rule in Eqn (24). Instead these nodes retain the support radius associated with the larger spacing. For example, in Figure 3, without the extra nodes, node A would have a support radius of ah. Due to the extra nodes, node B in particular, the support radius of node A would be given by $ah/2$ according to Eqn (24). We ignore this, and leave node A with a support radius of ah. Therefore a structured nodal arrangement is combined with a variable rule for nodal support. This has implications for adaptive re–gridding in meshless methods which will be highlighted later.

Table 1: The residual force for several load steps.

normalised residual force				
iteration number	load step number 26	27	28	29
1	2.7540E-01	3.9499E-01	5.3573E-01	5.6752E-01
2	7.5770E-02	6.7376E-02	6.2604E-02	1.4941E-01
3	6.9034E-03	2.2317E-03	6.5026E-03	1.0072E-02
4	6.9047E-06	7.9570E-07	1.4430E-06	3.0972E-05
5	1.4239E-11		4.2575E-11	1.3345E-11

The performance of this scheme is demonstrated using the same (flexible) footing problem as above. The parameters used are summarized in Table 2. Figures 4, 5 and 6 show the normalised load–displacement response using the hierarchical arrangement for 181, 485 and 980 nodes in the meshless near field. We see that for certain values of the nodal support parameter a convergence to the limit load is not possible. However generally the ability of the meshless formulation to reach the limit load is much improved over the uniform arrangements. The results suggest that with the nodal arrangement specified (i.e. subdivisions by one–half and one quarter at the domain corners), the optimum value for the nodal support parameter is $a = 2.5 - 3.0$. This is in contrast to the much larger upper limit on this parameter suggested by other authors and mentioned above. Figure 7 shows the progress of convergence for an example analysis in this series. Figure 7(a) shows the out-of-balance (or residual) load at each iteration step showing the increasing

Table 2: Parameters used in the numerical simulations

Material Parameters	$E = 1000$, $\nu = 0.25$, $c_u = 0.3$ von Mises and Trecsa yield surfaces used	
MLPG parameters	domain size	$[0,\infty) \times (-\infty,3]$
	2D meshless domain	$[0,3] \times [0,3]$
	d_{min}	calculated by the code; the distance between a node and its nearest neighbour
	r_{supp}	$r_{supp} \in [2d_{min}, 4d_{min}]$
	r_{test}	d_{min} or $1.5d_{min}$
	nodes (meshless)	181, 485, 980
	nodes (in total)	198, 518, 1031
	order of basis	quadratic
	weight function	a quartic spline, given in Equation (23)

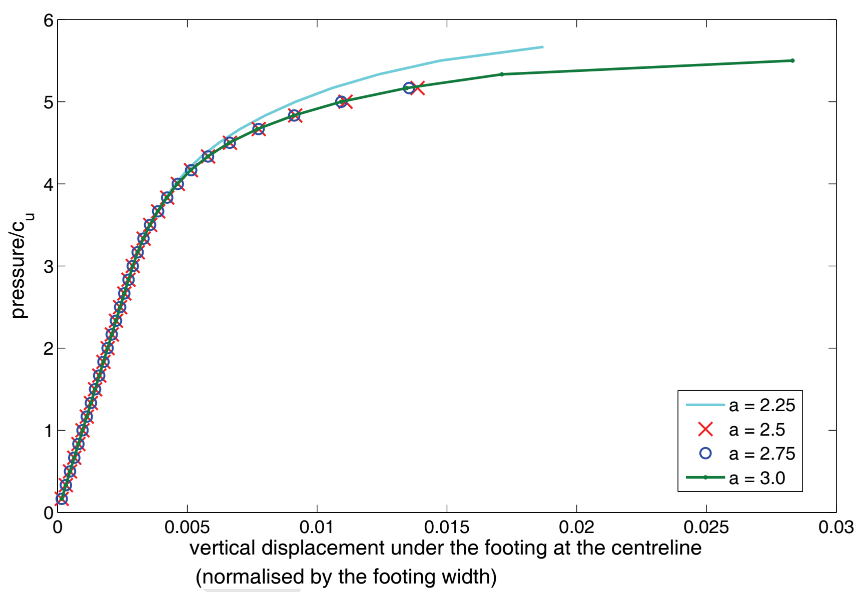

Figure 4: Load displacement curves for the hierarchical arrangement using 181 nodes and the test radius given by Eqn (24) with $b = 1.5$.

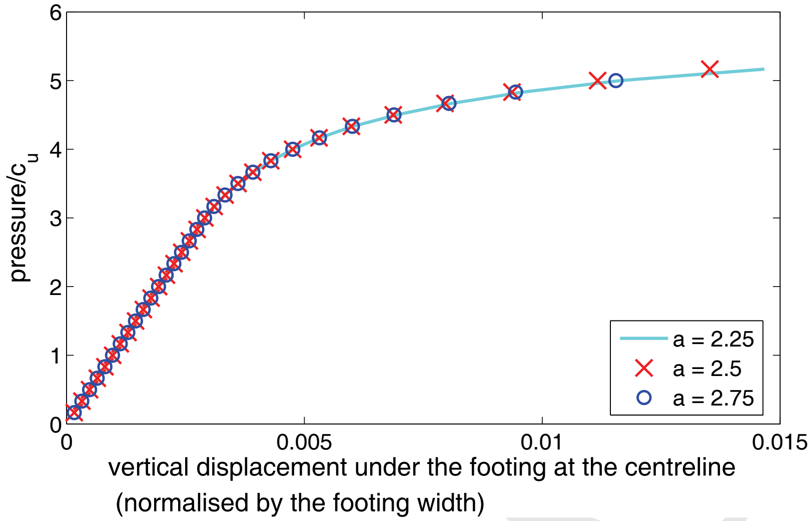

Figure 5: Load displacement curves for the hierarchical arrangement e using 485 nodes and $b = 1.5$

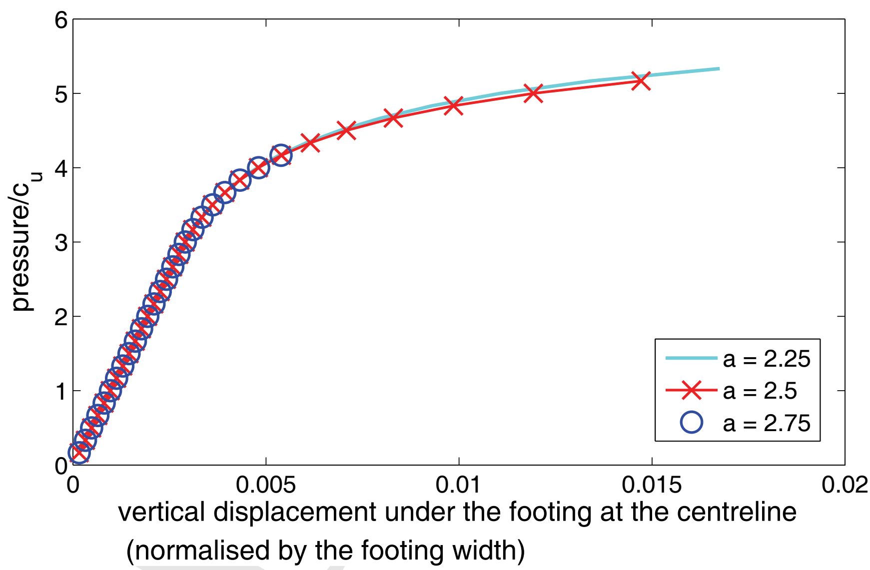

Figure 6: Load displacement curves for the hierarchical arrangement using 980 nodes and $b = 1.5$.

values until a failure to converge, while Figure 7(b), on a semilog plot shows the expected quadratic convergence of the Newton Raphson solver for each out-of-balance force vector. From Table 1 we can see that during a load step the residual force at a particular iteration is approximately equal to the square of the residual force at the previous iteration. This demonstrates the quadratic convergence of the global Newton–Raphson scheme. Figure 8 shows the surface displacement for an example analysis for a sequence of load steps. The ability to model the movements of a flexible footing at the surface is clear in this plot. The progressive expansion of the plastic region under the footing is modelled accurately by this method as demonstrated in Figure 9. Points that have just reached the yield surface are shown in orange, while those that reached it in a previous load step are red. The plot shows the development of the usual "bulb" of yielded material beneath the footing and its expansion as the load increases. To guarantee coverage, $r_{test} \geqslant d_{min}/\sqrt{2}$, or $b \geqslant 1/\sqrt{2}$. Two values of b have been tested, $b = 1$ and $b = 1.5$. For $b = 1$ Figure 10 (upper plot) shows that on varying the support radius, the load displacement curve varies significantly. However, for the larger test radius of $b = 1.5$, Figure 10 (lower plot) shows that changing the support radius has almost no impact on the profile of the load displacement curve.

For comparison on these plots we also show the load–displacement response using finite elements. The finite element parameters are as follows: the domain measures 12×5. At the truncated edges boundary conditions are applied that fix both the horizontal and vertical displacements. The footing half–width is 2 and the domain is covered by 32 quadratic quadrilateral elements. An arc–length method was used in order to obtain the limit load. The material parameters used are the same as those used in the meshless simulations and are given in Table 2. The response of the finite element model is always stiffer than the meshless results however this is due to the coarseness of the finite element mesh used here.

To demonstrate that the elasto-plastic MLPG region could be used on its own, same code is used to solve the governing equations for the finite region ("MLPG zone" in Figure 1(b)) alone with essential boundary conditions applied along the boundary between the MLPG and scaled boundary zones (the latter being removed entirely). In Figure 11 the FEM results are compared with results from the meshless code solving the problem on the MLPG zone and also with the results from the hybrid MLPG method (i.e. including the scaled boundary zone). It can be seen that the meshless results from the finite domain have a steeper elastic response than the results from the hybrid code on the semi–infinite domain, as might be expected given the imposition of essential boundaries a finite distance from the loading in the former. The responses of the meshless models are still not as stiff as the FE results however due again to the coarseness of the FE grid.

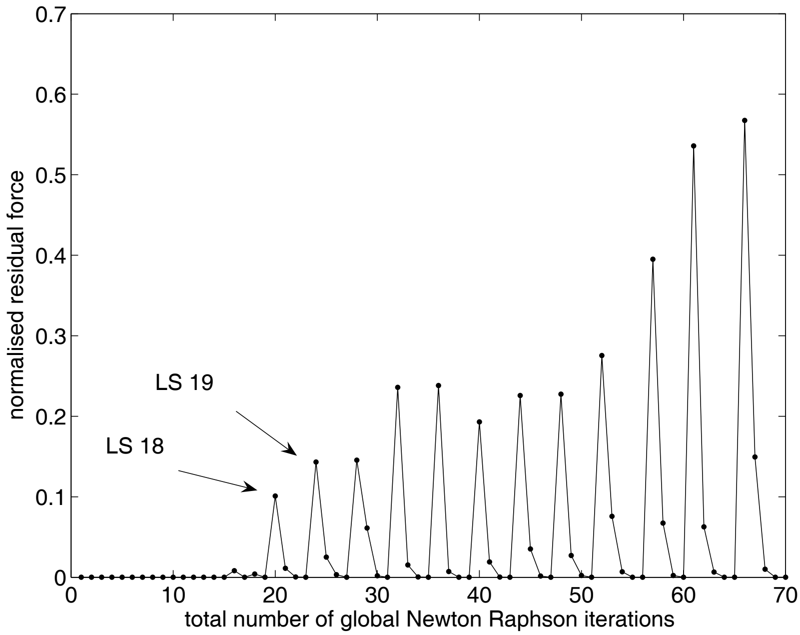

(a)

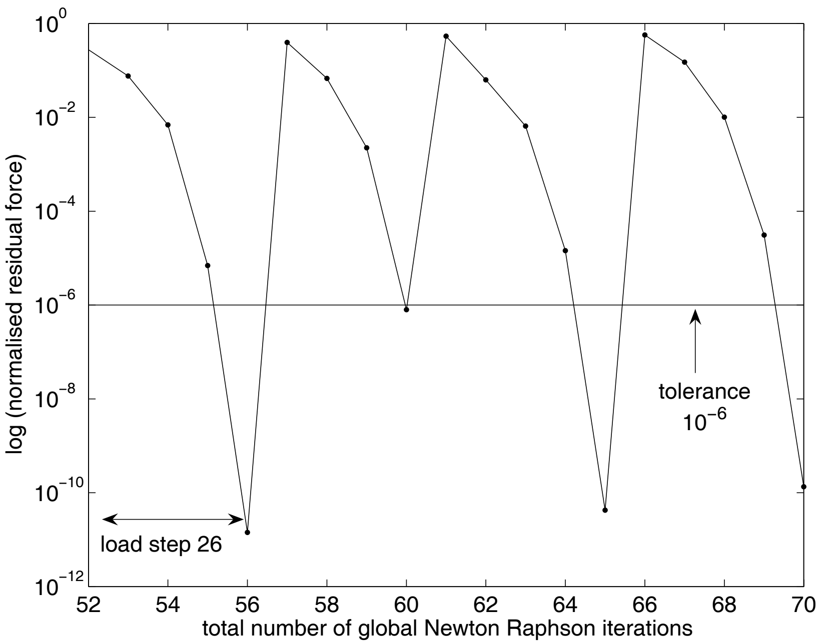

(b)

Figure 7: Convergence patterns of the global NR scheme (485 meshless nodes / 518 nodes in total and $a = 2$).

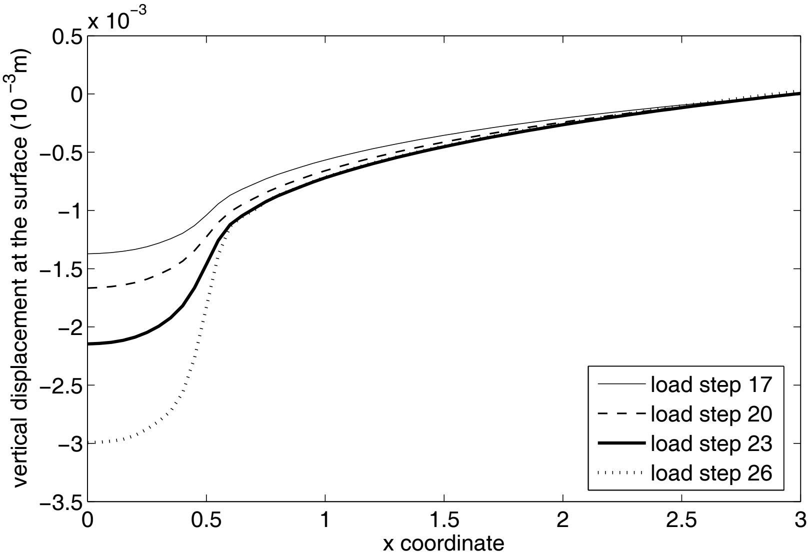

Figure 8: Plots of surface vertical displacement for several load steps.

These results provide sufficient evidence that elasto–plasticity can be accurately modelled using the hybrid MLPG method but also demonstrate the need for a careful choice of nodal arrangement and support radius rules. The implications for adaptive refinement in meshless methods are that merely inserting nodes without changing the nodal support radius rule could actually make the solution less optimal rather than improving it, unless the nodal support rules are also varied. The hierarchical approach is necessary here due to the proximity of the boundaries; at a corner there are two boundaries and therefore the nodal arrangement needs to be more refined but also the nodal support rules have to be changed. If we were to refine the mesh based on some measure of error estimation, this would be an additional consideration and it will be interesting to see if the two requirements compete or are complementary.

4 Conclusions

Meshless methods remove the need for a mesh to be generated in order to solve problems in elasto–plasticity, thereby having strong potential for their future use in very large 3D simulations and in problems for which successive remeshing would be necessary, as in those involving large deformations. Before we can get to that point however, these methods need to be proved on problems that are well–within

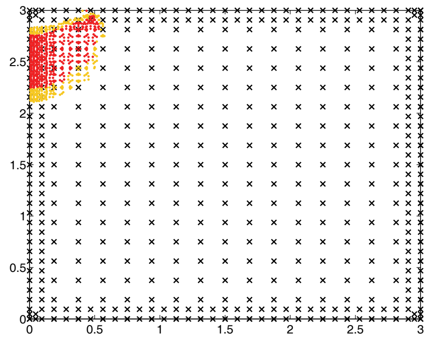

(a) Load step 20

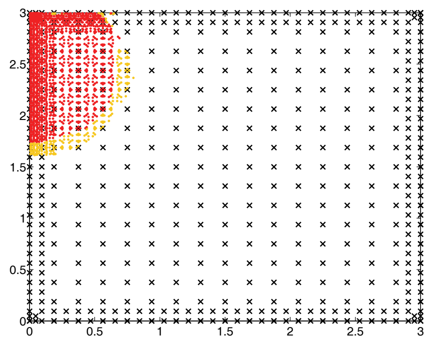

(b) Load step 24

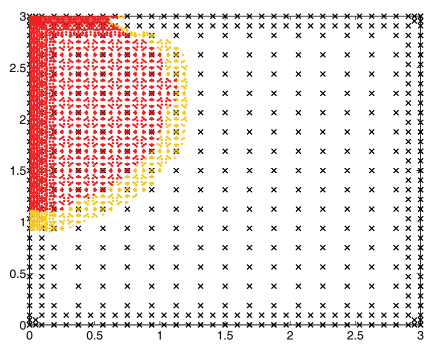

(c) Load step 28

Figure 9: Plastic zone at several load steps. (Integration points that have become plastic at the current load step are in orange, those points that were already plastic are marked in red.)

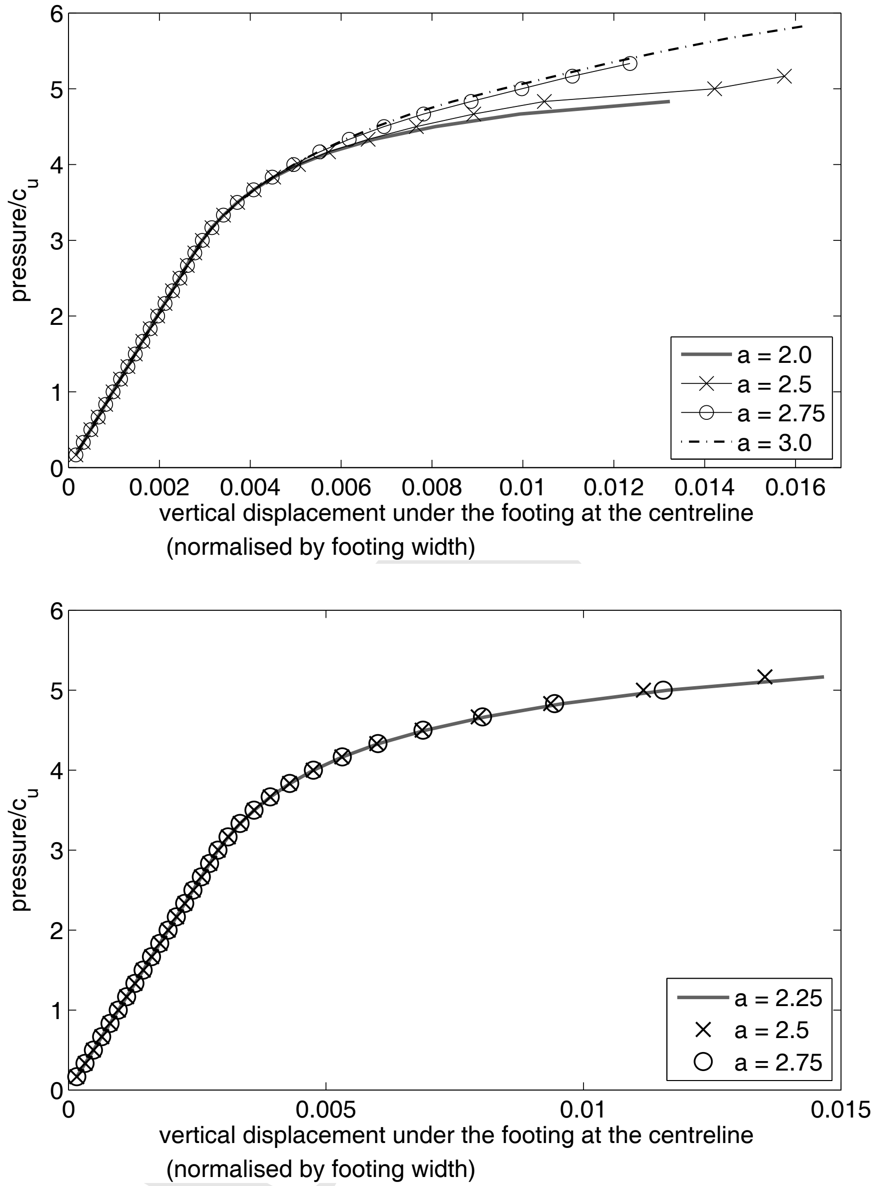

Figure 10: Load displacement curves for the hierarchical arrangement using 485 meshless nodes showing a range of support radii. Above r_{test} with $b = 1$, below $b = 1.5$

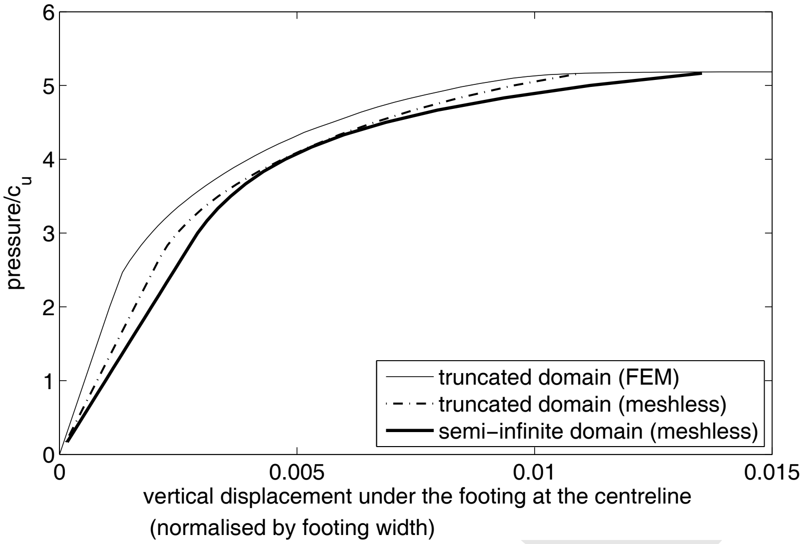

Figure 11: Load displacement curves comparing FEM results from a truncated domain with meshless results from a truncated domain and a semi-infinite domain (for $b = 1.5$, 485 meshless nodes).

the capabilities of the conventional finite element method. In this study we have shown that the MLPG method is sensitive to a number of user–defined features of a simulation. Firstly the distribution of nodes has been shown to be very important for the accurate determination of stresses and for the success of an incremental scheme. Secondly the choice of nodal support rule has a major effect both on accuracy and robustness using elasto–plasticity. Both of these points should not unnecessarily deter modellers from using these methods, for the potential future advantages mentioned above. However, the results of this study indicate that care is necessary at all stages.

Acknowledgement: The research is funded by the UK EPSRC grant EP/D07711-/01. The authors thank Dr M.E. Honnor of Bradford University for the use of FE results of footing problems.

References

Andreaus, U.; Batra, R.; Porfiri, M. (2005): Vibrations of cracked Euler-Bernoulli beams using Meshless Local Petrov-Galerkin (MLPG) method. *CMES-*

Comp. Model Eng., vol. 9, no. 2, pp. 111–131.

Askes, H.; de Borst, R.; Heeres, O. (1999): Conditions for locking-free elasto-plastic analyses in the Element-Free Galerkin method. *Comput. Methods Appl. Mech. Engrg.*, vol. 173, no. 1-2, pp. 99–109.

Atluri, S.; Liu, H.; Han, Z. (2006): Meshless Local Petrov-Galerkin (MLPG) Mixed Finite Difference Method for Solid Mechanics . *CMES-Comp. Model. Eng.*, vol. 15, pp. 1–16.

Atluri, S. N.; Shen, S. P. (2002): The meshless local Petrov-Galerkin (MLPG) method: A simple & less-costly alternative to the finite element and boundary element methods. *CMES-Comp. Model Eng.*, vol. 3, no. 1, pp. 11–51.

Atluri, S. N.; Zhu, T. (1998): A new meshless local Petrov-Galerkin (MLPG) approach in computational mechanics. *Comput. Mech.*, vol. 22, pp. 117–127.

Barry, W.; Saigal, S. (1999): A three-dimensional element-free Galerkin elastic and elastoplastic formulation. *Int. J. Numer. Meth. Eng.*, vol. 46, no. 5, pp. 671–693.

Batra, R. C.; Porfiri, M. (2008): Analysis of rubber-like materials using meshless local Petrov-Galerkin (MLPG) method. *Commun. Numer. Meth. En.*, vol. 24, no. 12, Sp. Iss. SI, pp. 1781–1804.

Belinha, J.; Dinis, L. M. (2006): Elasto-plastic analysis of plates by the element free Galerkin method. *Eng. Comp.*, vol. 23, no. 5-6, pp. 525–551.

Belytschko, T.; Lu, Y. Y.; Gu, L. (1994): Element-free Galerkin methods. *Int. J. Numer. Meth. Eng.*, vol. 37, pp. 229–256.

Bergamaschi, L.; Martinez, A.; Pini, G. (2009): An Efficient Parallel MLPG Method for Poroelastic Models. *CMES-Comp. Model Eng.*, vol. 49, no. 3, pp. 191–215.

Deeks, A.; Augarde, C. (2005): A meshless local Petrov-Galerkin scaled boundary method. *Comput. Mech.*, vol. 36, pp. 159–170.

Deeks, A. J.; Augarde, C. E. (2007): A hybrid meshless local Petrov-Galerkin method for unbounded domains. *Comput. Methods Appl. Mech. Engrg.*, vol. 196, no. 4-6, pp. 843–852.

Feng, W. J.; Han, X.; Li, Y. S. (2009): Fracture Analysis for Two-dimensional Plane Problems of Nonhomogeneous Magneto-electro-thermo-elastic Plates Subjected to Thermal Shock by Using the Meshless Local Petrov-Galerkin Method. *CMES-Comp. Model Eng.*, vol. 48, no. 1, pp. 1–26.

Fernández-Méndez, S.; Huerta, A. (2004): Imposing essential boundary conditions in mesh-free methods. *Comput. Methods Appl. Mech. Engrg.*, vol. 193, pp. 1257–1275.

Fries, T.; Matthies, H. (2004): Classification and overview of meshfree methods. Technical Report 2003-3, Technical University Braunschweig, Brunswick, Germany, 2004.

Han, Z.; Atluri, S. (2004): Meshless Local Petrov-Galerkin (MLPG) approaches for solving 3D Problems in elasto-statics. *CMES-Comp. Model. Eng.*, vol. 6, pp. 169–188.

Han, Z.; Rajendran, A.; Atluri, S. (2005): Meshless Local Petrov-Galerkin (MLPG) approaches for solving nonlinear problems with large deformations and rotations. *CMES-Comp. Model Eng.*, vol. 10, no. 1, pp. 1–12.

Hazama, O.; Okuda, H.; Wakatsuchi, K. (2001): A digital systematization of meshfree method and its applications to elasto-plastic infinitesimal deformation analysis. *Adv. Eng. Softw.*, vol. 32, no. 8, pp. 647–664.

Hill, R. (1950): *The Mathematical Theory of Plasticity*. Clarendon Press, Oxford.

Jarak, T.; Soric, J. (2008): Analysis of rectangular square plates by the mixed Meshless Local Petrov-Galerkin (MLPG) approach. *CMES-Comp. Model Eng.*, vol. 38, no. 3, pp. 231–261.

Kargarnovin, M.; Toussi, H.; Fariborz, S. (2004): Elasto-plastic element-free Galerkin method. *Comput. Mech.*, vol. 33, no. 3, pp. 206–214.

Kasper, T.; Meschke, G. (2004): A 3D finite element simulation model for TBM tunnelling in soft ground. *Int. J. Numer. Anal. Methods Geomech.*, vol. 28, no. 14, pp. 1441–1460.

Lancaster, P.; Salkauskas, K. (1981): Surfaces generated by moving least squares methods. *Math. Comput.*, vol. 37, pp. 141–158.

Liu, W.; Jun, S.; Li, S.; Adee, J.; Belytschko, T. (1995): Reproducing kernel particle methods for structural dynamics. *Int. J. Numer. Meth. Eng.*, vol. 38, no. 10, pp. 1655–1679.

Long, S. Y.; Liu, K. Y.; Li, G. Y. (2008): An analysis for the elasto-plastic fracture problem by the meshless local Petrov-Galerkin method. *CMES-Computer Modeling in Engineering & Sciences*, vol. 28, no. 3, pp. 203–216.

Monaghan, J. (1988): An introduction to SPH. *Comput. Phys. Comm.*, vol. 48, pp. 89–96.

Nayroles, B.; Touzot, G.; Villon, P. (1992): Generalizing the finite element method: diffuse approximation and diffuse elements. *Comput. Mech.*, vol. 10, pp. 307–318.

Nguyen, V. P.; Rabczuk, T.; Bordas, S.; Duflot, M. (2008): Meshless methods: A review and computer implementation aspects. *Math. Comput. Simulat.*, vol. 79, no. 3, pp. 763 – 813.

Nie, Y.; Atluri, S.; Zuo, C. (2006): The optimal radius of the support of radial weights used in moving least squares approximation. *CMES-Comp. Model Eng.*, vol. 12, pp. 137–147.

Pamin, J.; Askes, H.; de Borst, R. (2003): Two gradient plasticity theories discretized with the element-free Galerkin method. *Comput. Methods Appl. Mech. Engrg.*, vol. 192, no. 20-21, pp. 2377–2403.

Pannachet, T.; Askes, H. (2000): Some observations on the enforcement of constraint equations in the EFG method. *Commun. Numer. Methods Eng.*, vol. 16, no. 12, pp. 819–830.

Pini, G.; Mazzia, A.; Sartoretto, F. (2008): Accurate MLPG solution of 3d potential problems. *CMES-Comp. Model. Eng.*, vol. 36, pp. 43–64.

Seyrafian, S.; Gatmiri, B.; Noorzad, A. (2007): Analytical Investigation of Depth Non-homogeneity Effect on the Dynamic Stiffness of Shallow Foundations. *CMES-Comp. Model. Eng.*, vol. 21, pp. 209–217.

Sheng, D.; Nazem, M.; Carter, J. P. (2009): Some computational aspects for solving deep penetration problems in geomechanics. *Comput. Mech.*, vol. 44, no. 4, pp. 549–561.

Simo, J. C.; Hughes, T. J. R. (1998): *Computational Inelasticity*. Interdisciplinary Applied Mathematics: Mechanics and Materials. Springer.

Sladek, J.; Sladek, V.; Krivacek, J.; Wen, P. H.; Zhang, C. (2007): Meshless local Petrov-Galerkin (MLPG) method for Reissner-Mindlin plates under dynamic load. *Comput. Method. Appl. M.*, vol. 196, no. 25-28, pp. 2681–2691.

Sladek, J.; Sladek, V.; Solek, P. (2009): Elastic analysis in 3D anisotropic functionally graded solids by the MLPG. *CMES-Comp. Model Eng.*, vol. 43, no. 3, pp. 223–251.

Sladek, J.; Sladek, V.; Solek, P.; Atluri, S. (2008): Modeling of Intelligent Material Systems by the MLPG. *CMES-Comp. Model. Eng.*, vol. 34, pp. 273–300.

Sladek, J.; Sladek, V.; Solek, P.; Pan, E. (2008): Fracture analysis of cracks in magneto-electro-elastic solids by the MLPG. *Comput. Mech.*, vol. 42, no. 5, pp. 697–714.

Sladek, J.; Sladek, V.; Solek, P.; Tan, C. L.; Zhang, C. (2009): Two- and Three-Dimensional Transient Thermoelastic Analysis by the MLPG Method. *CMES-Comp. Model. Eng.*, vol. 47, no. 1, pp. 61–95.

Soares, D.; Sladek, J.; Sladek, K. (2009): Dynamic Analysis by Meshless Local Petrov-Galerkin Formulations Considering a Time-Marching Scheme Based on Implicit Green's Functions. *CMES-Comp. Model. Eng.*, vol. 50, pp. 115–140.

Sterk, M.; Trobec, R. (2008): Meshless solution of a diffusion equation with parameter optimization and error analysis. *Eng. Anal. Bound. Elem.*, vol. 32, pp. 567–577.

Wang, L.; Daniewicz, S.; Horstemeyer, M.; Sintay, S.; Rollett, A. (2009): Three-dimensional finite element analysis using crystal plasticity for a parameter study of fatigue crack incubation in a 7075 aluminum alloy. *Int. J. Fatigue*, vol. 31, no. 4, pp. 659 – 667.

Wu, C.; Chen, J.; Chi, L.; Huck, F. (2001): Lagrangian meshfree formulation for analysis of geotechnical materials. *J. Eng. Mech-ASCE*, vol. 127, no. 5, pp. 440–449.

Xiong, Y. B.; Long, S. Y.; Liu, K. Y.; Li, G. Y. (2006): A meshless local Petrov-Galerkin method for elasto-plastic problems. In Liu, GR and Tan, VBC and Han, X(Ed): *Computational Methods, Pts 1 and 2*, pp. 1477–1482. 1st International Conference on Computational Methods (ICCM04), Singapore, Dec 15-17, 2004.

Zhuang, X.; Augarde, C. E. (2010): Aspects of the use of orthogonal basis functions in the element free Galerkin method. *Int. J. Numer. Meth. Eng.*, vol. 81(3), pp. 366–380.

493